Evolution from modal to spatially incoherent emission of a broad-area VCSEL

Shyam K. Mandre,[1,3] Wolfgang Elsäßer,[1] Ingo Fischer,[2,4] Michael Peeters,[2,5] and Guy Verschaffelt[2]

[1]*Institute of Applied Physics, Darmstadt University of Technology, Schloßgartenstr. 7, D-64289 Darmstadt, Germany*

[2]*Department of Applied Physics and Photonics, Vrije Universiteit Brussel, Pleinlaan 2, B-1050 Brussels, Belgium*

[3]*Now with: Braun GmbH, Frankfurter Str. 145, 61476 Kronberg, Germany*

[4]*Now with: School of Engineering and Physical Sciences and Joint Research Institute for Integrated Sytems, Heriot-Watt University, Edinburgh EH14 4AS, UK*

[5]*Now with: Alcatel-Lucent, Copernicuslaan 50, 2018 Antwerpen, Belgium*

Corresponding author: guy.verschaffelt@vub.ac.be

Abstract: Broad-area vertical-cavity surface-emitting lasers (BA-VCSELs) can exhibit a state of spatially incoherent emission, as we recently reported in [M. Peeters et al., Opt. Express, **13**, 9337 (2005)]. Here, we experimentally study the evolution of a BA-VCSEL under pulsed operation from well-defined modal emission with a multitude of transverse cavity modes to such spatially incoherent emission. The transition is studied using a high-speed intensified CCD camera and differential image analysis with which single-shot measurements of the imaged nearfield, farfield, spatial coherence, and spectral emission properties are acquired. This combination of experimental characterization tools allows for a detailed description of the BA-VCSEL's emission behavior, which is necessary for an in-depth understanding of the processes involved. We find the interplay between the thermal chirp and the build-up of a spatially distributed thermal lens to be decisive for the break-up of the global cavity modes.

OCIS codes: (140.7260) Vertical cavity surface emitting lasers; (030.1640) Coherence; (030.4070) Modes; (190.3100) Instabilities and chaos.

References and links

1. A. Haglund, J.S. Gustavsson, J. Vukusic, P. Modh, and A. Larsson, "Single Fundamental-Mode Output Power Exceeding 6 mW From VCSELs With a Shallow Surface Relief," IEEE Photon. Technol. Lett. **16,** 368–370 (2004).
2. C. J. Chang-Hasnain, M. Orenstein, A. Von Lehmen, L. T. Florez, J. P. Harbison, and N. G. Stoffel, "Transverse mode characteristics of vertical cavity surface-emitting lasers," Appl. Phys. Lett. **57**, 218–220 (1990).
3. C. Degen, I. Fischer, and W. Elsäßer, "Transverse modes in oxide confined VCSELs: influence of pump profile, spatial hole burning, and thermal effects," Opt. Express **5**, 38–47 (1999).
4. A. Valle, J. Sarma, and K. A. Shore, "Dynamics of transverse mode competition in vertical cavity surface emitting laser diodes," Opt. Commun. **115**, 297–302 (1995).

#89583 - $15.00 USD Received 9 Nov 2007; revised 8 Jan 2008; accepted 8 Jan 2008; published 18 Mar 2008

5. M. Giudici, J. R. Tredicce, G. Vaschenko, J. J. Rocca, and C. S. Menoni, "Spatio-temporal dynamics in vertical cavity surface emitting lasers excited by fast electrical pulses," Opt. Commun. **158**, 313–321 (1998).
6. J. Mulet and S. Balle, "Transverse mode dynamics in vertical-cavity surface-emitting lasers: spatiotemporal versus modal expansion descriptions," Phys. Rev. A **66**, 053 802 (2002).
7. A. Barchanski, T. Gensty, C. Degen, I. Fischer, and Elsäßer, "Picosecond emission dynamics of vertical-cavity surface-emitting lasers: spatial, spectral, and polarization-resolved characterization," IEEE J. Quantum Electron. **39**, 850–858 (2003).
8. K. Becker, I. Fischer, and W. Elsäßer, "Spatio-temporal emission dynamics of VCSELs: modal competition in the turn-on behavior," in *Proceedings of SPIE*, D. Lenstra, G. Morthier, T. Erneux, and M. Pessa, eds., **5452**, 452 (2004).
9. P. Debernardi, G. P. Bava, C. Degen, I. Fischer, and Elsäßer, "Influence of anisotropies on transverse modes in oxide-confined VCSELs," IEEE J. Quantum Electron. **38**, 73–84 (2002).
10. M. Peeters, G. Verschaffelt, H. Thienpont, S. K. Mandre, I. Fischer, and M. Grabherr, "Spatial decoherence of pulsed broad-area vertical-cavity surface-emitting lasers," Opt. Express **13**, 9337–9345 (2005).
11. F. Zernike, "The concept of degree of coherence and its application to optical problems," Physica **5**, 785–795 (1938).
12. A. C. Schell, "A technique for the determination of the radiation pattern of a partially coherent aperture," IEEE Trans. Antennas Propag. **AP-15**, 187–188 (1967).
13. E. Collett and E. Wolf, "Is complete spatial coherence necessary for the generation of highly directional light beams," Opt. Lett. **2**, 27–29 (1978).
14. L. Mandel and E. Wolf, *Optical Coherence and Quantum Optics* (Cambridge Univ. Pr., 1995).
15. S. K. Mandre, W. Elsäßer, I. Fischer, M. Peeters, and G. Verschaffelt, "Determining the temporally and radially resolved temperature distribution inside a pulsed broad-area vertical-cavity surface-emitting laser cavity," Appl. Phys. Lett. **89**, 151 106 (2006).
16. L. Wang and Q. Lin, "The evolutions of the spectrum and spatial coherence of laser radiation in resonators with hard apertures and phase modulation," IEEE J. Quantum Electron. **39**, 749–758 (2003).

1. Introduction

Over the last 20 years, some attractive emission properties of vertical-cavity surface-emitting lasers (VCSELs) compared to edge-emitting semiconductor lasers have led to VCSELs' establishment as a prominent device within the semiconductor laser family. These properties include near-circular beam profiles, in contrast to astigmatic beams emitted by edge-emitting SLs. A further property of VCSELs, resulting from their short cavities, is single longitudinal mode emission. For a small enough aperture diameter (typically less than $\sim$5 μm) the emission can even be in a single, fundamental transverse mode with an output power up to 7 mW [1]. VCSELs find application in different fields, most noteworthy in data-communication and optical sensing. For other applications, such as printing or projection systems, higher output powers are required. This can be achieved by increasing the VCSELs' aperture diameter up to 100 μm. With these larger devices, CW output powers up to 100 mW are attainable. However, the large Fresnel number of these broad-area VCSELs (BA-VCSELs) typically leads to the onset of a multitude of higher order transverse modes [2, 3]. This results in a structured and more divergent farfield (FF) beam profile, thus deteriorating the beam quality of the emitted light. The multi-transverse mode emission is accompanied by complex emission dynamics, which can be observed as a combination of spatiotemporal and polarization dynamics. The build-up of transverse modes, the spatiotemporal emission dynamics, and the interplay of the responsible mechanisms have been studied previously [4, 5, 6, 7, 8, 9].

We recently demonstrated that next to the well-known modal emission, BA-VCSELs in pulsed operation can exhibit a state of nonmodal, or spatially incoherent emission [10]. In the case of modal emission, the cavity modes are determined by the geometric properties of the devices and the interaction between the light and the semiconductor material. The total emission maintains a considerable degree of spatial coherence because of the inherent coherence of each individual mode. In contrast, the spatially incoherent emission may be associated with emission in independent "coherence islands" with dimensions of a few micron, thus, neglecting the global boundary conditions defined by the device's structure. As the coherence radius of the

#89583 - $15.00 USD Received 9 Nov 2007; revised 8 Jan 2008; accepted 8 Jan 2008; published 18 Mar 2008

BA-VCSELs in the case of incoherent emission has been found to be much smaller than the aperture dimensions, the BA-VCSELs can be considered as "quasi-homogeneous Schell-model sources" [11, 12, 13, 14]. If the FF intensity distribution of a Schell-model source exhibits a Gaussian profile, then the complex coherence function also has to be a Gaussian with a width inversely proportional to the width of the FF intensity profile [10, 13, 14]. The BA-VCSEL studied in [10] exhibits such an incoherent, Gaussian FF profile under a wide range of operating conditions. Such high power, spatially incoherent sources can be useful in projection systems as the low degree of spatial coherence might help to reduce the speckle contrast. However, the details of the incoherent emission's emergence and the underlying mechanisms have been unclear so far. This knowledge is crucial in order to design appropriate sources and to potentially transfer the concept to other lasers.

The measurements in [10] also suggested that the occurrence of incoherent emission is a dynamic effect characterized by a dynamic evolution from modal to incoherent emission during a pulse. This is not a transition between two stationary states, i.e. between states that exist without any change in the control parameters: in the incoherent emission regime the modes of the VCSEL cavity are prevented to build-up and the cavity is kept in a transient state. In this paper, we will address this dynamic transition between the modal and the spatially incoherent state of emission of a 50 μm BA-VCSEL. To do so, we will use a combination of different experimental techniques. We will present single-shot measurements of the BA-VCSEL's emission dynamics using a high-speed intensified CCD camera with a temporal resolution of 300 ps. Single-shot measurements of the imaged nearfield (NF) and FF emission, and of the spectrally dispersed NF profiles will demonstrate that the BA-VCSEL initially (during the turn-on process) exhibits modal emission. Only after a few hundred nanoseconds, the BA-VCSEL's emission exhibits the transition towards a Gaussian FF profile. We will show that the appearance of the Gaussian FF is associated with a drastic drop in the spatial coherence. The spectrally dispersed NF profiles are further complemented by measurements of the RF spectrum of the intensity fluctuations. When the Gaussian FF is established, we observe a flat, non-peaked RF spectrum in accordance with the assumption of having non-modal emission. Finally, we will demonstrate how the modal emission reappears after a few tens of microseconds.

2. Characterization of the BA-VCSEL's emission profile

2.1. Device characteristics

For our measurements we use an oxide confined BA-VCSEL with an aperture diameter of 50 μm. The BA-VCSEL emits at a wavelength of $\sim$840 nm with a maximum cw output power of $\sim$70 mW at an injected current of 80 mA. The VCSEL's threshold current I_{thr} is approximately 14 mA. The experimental setup is modified depending on the measurement performed and will be discussed in the corresponding paragraphs.

2.2. Setup

The BA-VCSEL's emission is recorded by a 10-bit, fast-gated intensified CCD-camera (iCCD, *4picos, Stanford Computer Optics, Inc.*) with an exposure time of 300 ps. We can therefore observe the emission dynamics of the BA-VCSEL and the processes responsible for the observed emission behavior on these short ps timescales. The camera is used to trigger a pulse generator and, subsequently, the BA-VCSEL at 50 Hz. The pulse widths with which we drive the BA-VCSEL are chosen between 10 and 100 μs. With the resulting low duty cycle of less than 0.5%, we can assume that the VCSEL cools down to the sub-mount temperature (set at 28 °C) before the consecutive pulse is applied. Our setup allows us to acquire single-shot measurements at different temporal positions within the VCSEL-pulse by shifting the exposure gate-window

#89583 - $15.00 USD Received 9 Nov 2007; revised 8 Jan 2008; accepted 8 Jan 2008; published 18 Mar 2008

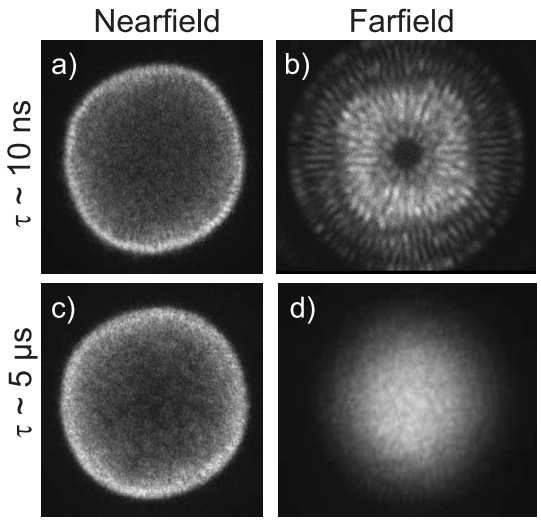

Fig. 1. Upper row: a) Nearfield intensity distribution and b) corresponding farfield intensity distribution, both at $\tau \sim 10$ ns. Bottom row: c) Nearfield intensity distribution and d) corresponding farfield intensity distribution, both at $\tau \sim 5$ μs. The pulse amplitude is 160 mA in all cases.

with an adjustable delay line. Therefore, we can study the evolution of the BA-VCSEL's emission during the entire pulse. To measure FF profiles of the emission, we place the camera at a distance of $\sim$2.5 cm from the laser facet. Alternatively, we acquire magnified NF profiles of the emission by inserting an imaging lens into the setup.

2.3. Nearfield - Farfield Comparison

Fig. 1 depicts single-shot measurements of the NF and corresponding FF intensity distributions at the onset of laser emission and after 5 μs. The measured profiles have been verified to be essentially the same for each pulse, therefore we can compare the NF and corresponding FF profiles even though they have not been measured simultaneously. We find that the BA-VCSEL's emission undergoes a radical change during the first microseconds after turn-on. Figure 1(a) depicts the NF intensity distribution at $\tau \sim 10$ ns, where τ is the time after the onset of laser emission. At this early stage of emission, the NF emission is dominated by ring-shaped high order Gauss-Laguerre modes (daisy-modes) emitted at the periphery of the VCSEL-aperture. The transverse modes are more clearly resolved in the corresponding FF profile at $\tau \sim 10$ ns in Fig. 1(b). The FF exhibits structured and divergent emission and reflects the highly multimode emission of the corresponding NF profile. The FF and NF at $\tau \sim 10$ ns are in agreement with the results obtained so far for multimode VCSELs [6, 7, 8].

In contrast, the measurements at $\tau \sim 5$ μs shown in Fig. 1(c) and (d) exhibit a significantly different behavior. The NF intensity distribution at $\tau \sim 5$ μs (see Fig. 1(c)) is similar and only slightly blurred compared to the NF profile at $\tau \sim 10$ ns. The NF at $\tau \sim 5$ μs again suggests that high-order transverse modes dominate the BA-VCSEL's emission. However, the corresponding FF profile at $\tau \sim 5$ μs does not confirm this assumption. Instead of a structured FF profile reflecting multi-mode emission , the FF in Fig. 1(d) exhibits a Gaussian intensity distribution. Moreover, while the structured FF profiles at the beginning of the emission [such as in Fig. 1(b)] can be obtained by Fourier transform of the corresponding NF profiles [such as in Fig. 1(a)], numerical analysis did not provide any phase profile with which the Gaussian FF profile such

#89583 - $15.00 USD Received 9 Nov 2007; revised 8 Jan 2008; accepted 8 Jan 2008; published 18 Mar 2008

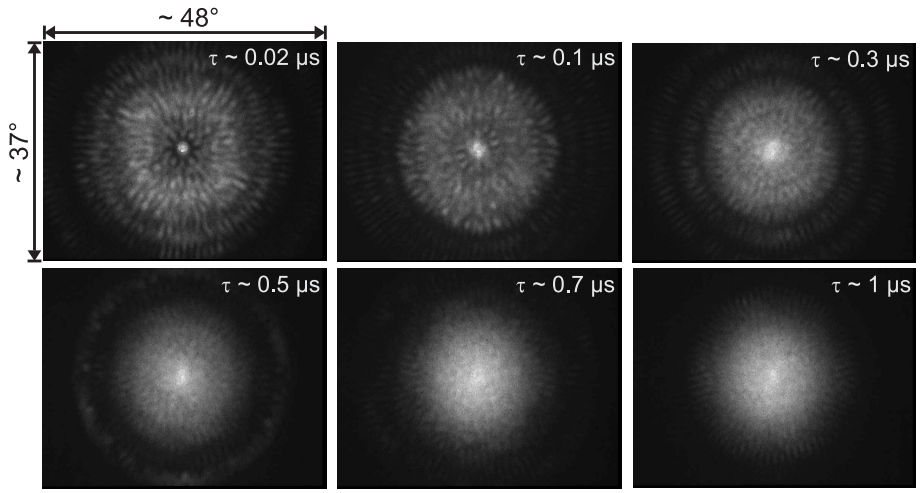

Fig. 2. Sequence of single-shot measurements of the BA-VCSEL's farfield emission behavior. The BA-VCSEL was operated in quasi-cw mode with pulse widths of 30 μs and pulse amplitude of 160 mA. The times denoted below the images are the temporal positions of the single-shot measurements after turn-on.

as in Fig. 1(d) could be constructed by Fourier transform of the corresponding NF such as in Fig. 1(c). The emission now corresponds to the spatially incoherent emission discussed in [10]. Because of the similarity between the NF profiles depicted in Figs. 1(a) at $\tau \sim 10$ ns and (c) at $\tau \sim 5$ μs, we can exclude significant changes in the carrier distribution from being responsible for the drastic change in the observed FF profile. In addition, the non-Gaussian NF profile in Fig. 1(c) proves that single, fundamental mode emission is not the origin of the Gaussian FF profile.

2.4. Farfield evolution

Given the two snapshots in Fig. 1, the question arises how the transition between these different emission regimes emerges and which processes are relevant for that. In the following we investigate this dynamical transition by measuring the temporally resolved FF at different temporal positions within a pulse. In Fig. 2 we depict a sequence of six single-shot measurements of the FF emission acquired at different times τ after onset of lasing emission. Initially, at $\tau \sim$20 ns, the BA-VCSEL's emission exhibits high order transverse mode emission similar to the FF profile at $\tau \sim$10 ns shown in Fig. 1 b). The full opening angle of the FF profile is approximately 35°. In addition, the FF profile at $\tau \sim$20 ns exhibits a narrow intensity peak in the center. The emission increasingly concentrates towards the center of the FF profile during the next 500 ns, while modal patterns can still be recognized at large angles. The FF emission after $\tau \sim 0.3$ μs shows more and more smearing of the modal patterns and increasing spatial homogeneity of the profiles. At $\tau \sim 1$ μs, the FF has evolved into a Gaussian profile with an emission angle of less than 20°. The Gaussian FF intensity distribution persists for several tens of microseconds, after which modal emission with a structured FF profile reappears. We note that this re-appearance of modes is consistent with the Gaussian FF profile not being observed in CW operation. Using a single-shot streak camera with a temporal resolution of $\sim$10 ps we investigated whether faster dynamics underlies the Gaussian profile. The streak camera measurements did not reveal such faster dynamics.

The FF profile thus exhibits a drastic change during the emitted pulse, whereas the changes

#89583 - $15.00 USD Received 9 Nov 2007; revised 8 Jan 2008; accepted 8 Jan 2008; published 18 Mar 2008

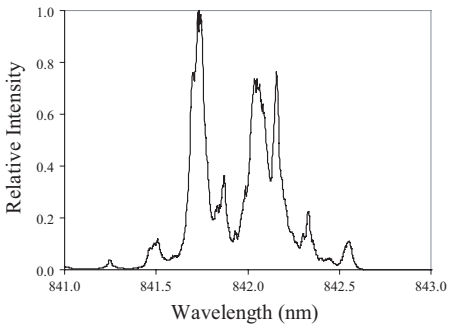

Fig. 3. Optical spectrum for a CW current of 60 mA.

observed in the NF intensity profiles are rather minor. The changes happen on a time-scale much slower than the photon and carrier lifetimes, indicating that other effects play a dominant role. To understand the responsible processes we will investigate the spectral evolution during the pulse.

3. Spectral Evolution

3.1. Spectrally dispersed NF

Before we look at the temporally resolved spectra during a pulse, we first plot in Fig. 3 the optical spectrum of the BA-VCSEL when it is driven by a CW current of 60 mA. This spectrum serves as a reference for the spectral measurements under pulsed conditions as presented below. In this optical spectrum, multiple groups of modes are clearly visible. The broad peaks in Fig. 3 (e.g. at 842.05 nm) indicate that some of the transverse modes are spectrally overlapping with each other. Not all of the modes can be resolved because of the limited resolution of the optical spectrum analyzer (0.01 nm or 4.25 GHz at a center wavelength of 842 nm).

To characterize the spectral content during a pulse, we measure the spectrally dispersed NF in a similar setup as the one used for the NF measurements but now the emission is also dispersed horizontally using a Czerny-Turner Imaging Spectrometer. Figure 4 shows a sequence of six such obtained single-shot measurements of the BA-VCSEL's spectrally dispersed NF. These images depict a spatial (radial) direction of the NF along the ordinate and the abscissa and an additional spectral dispersion of the NF along the abscissa. This experimental technique has the advantage of providing 2-dimensional spatial resolution with additional spectral resolution along the abscissa [15]. For these measurements, the VCSEL was driven by the same pump current as for the FF measurements of Fig. 2. Moreover, the temporal positions of the single-shot measurements depicted in Fig. 4 approximately correspond to those of the FF measurements of Fig. 2. At $\tau \sim$20 ns, high order multi-transverse modes are recognizable on the short-wavelength side of the spectrum. On the long-wavelength side, the spectrum exhibits a cloud of modes which are not resolved individually. During the next hundreds of nanoseconds, a qualitative change is visible in the spectral profiles. Whereas the individually resolved high-order modes on the short-wavelength side of the spectrum gradually disappear, the modes on the long-wavelength side transform into a parabola-like structure. This parabola-like structure is clearly visible at $\tau \approx 1\ \mu$s. Though ring-like structures can still be observed in the spectrum, we can not resolve any modes within the spectrum. Comparison of Figs. 2 and 4 reveals that the occurrence of the parabola-like structure in the spectrally dispersed NF coincides with the appearance of the Gaussian FF profile. The spectra confirm that single fundamental mode emission cannot be responsible for the occurrence of the Gaussian FF profile, as the fundamental

#89583 - $15.00 USD Received 9 Nov 2007; revised 8 Jan 2008; accepted 8 Jan 2008; published 18 Mar 2008

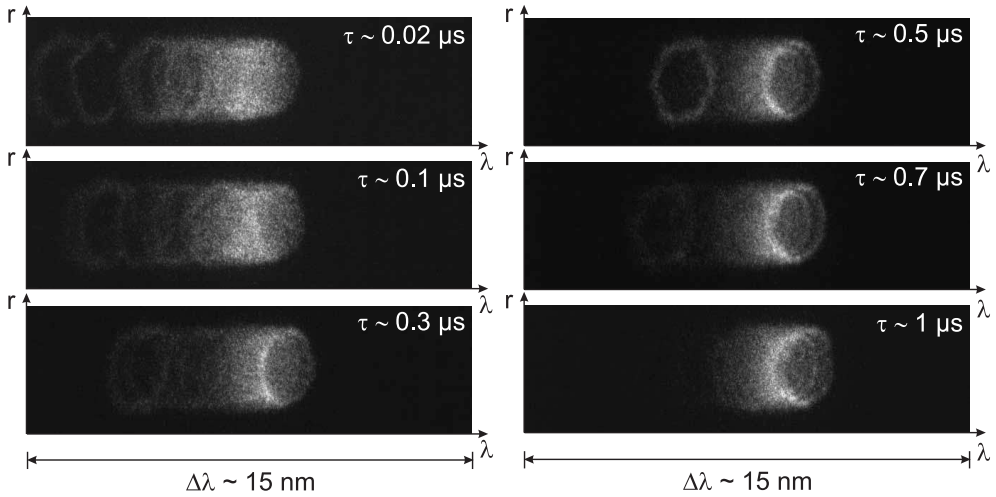

Fig. 4. Sequence of single-shot measurements of the BA-VCSEL's spectrally dispersed NF emission behavior. The BA-VCSEL was operated in quasi-cw mode with pulse widths of 30 μs and pulse amplitude of 160 mA. The times denoted in the upper right corner of the images are the positions of the single-shot measurements after turn-on. These temporal positions correspond approximately to the positions of the FF measurements in Fig. 2.

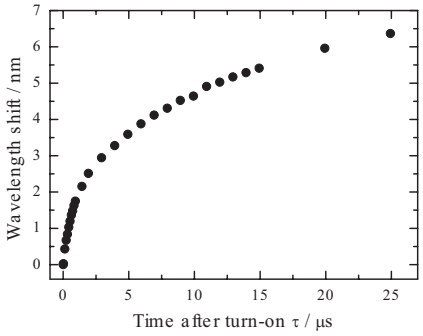

Fig. 5. Average wavelength shift of the BA-VCSEL's emission. The BA-VCSEL was operated in quasi-cw mode with pulse widths of 30 μs and pulse amplitude of 160 mA. The spectral positions were obtained by determining the intensity-weighted averages of the single-shot measurements at different τ.

mode does not appear in the optical spectra. The spectra in Fig. 4 also reveal a shift of the emission towards longer wavelengths during the first microsecond of the emitted pulse due to Joule heating. Figure 5 depicts the average wavelength shift during a 30 μs long pulse. The average wavelength at each temporal position is calculated as the intensity-weighted average over the corresponding single-shot spectrum of Fig. 4. Figure 5 shows that the emission wavelength shifts more than 6 nm within the first 25 microseconds of emission. The rate at which the wavelength shifts is clearly largest at the beginning of the pulse. The wavelength shift $\Delta\lambda$ can be approximated with a power law $\Delta\lambda(\tau_{turn-on}) = m\,\tau_{turn-on}^{b}$, where m is a scaling factor and the fitted value of b is 0.4.

#89583 - $15.00 USD Received 9 Nov 2007; revised 8 Jan 2008; accepted 8 Jan 2008; published 18 Mar 2008

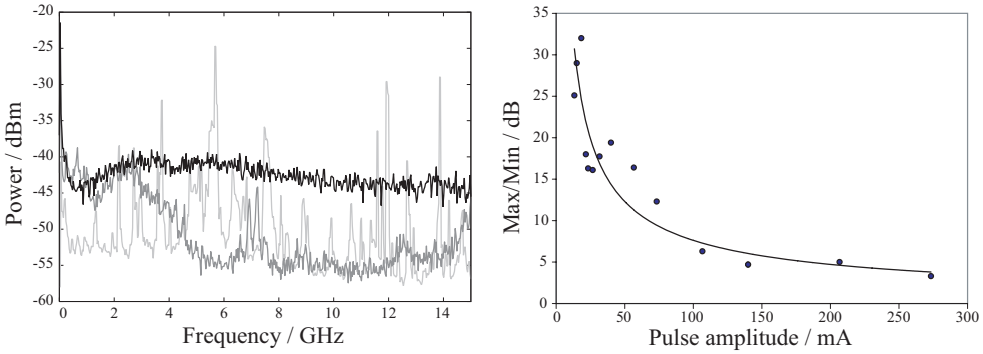

Fig. 6. Left: RF spectrum of the emitted intensity for CW, 70mA (light gray); and for 1 μs pulses with 1% duty cycle and 22 mA amplitude (dark gray) and 145 mA amplitude (black). The noise floor of the measurement setup is at -58 dBm. Right: Difference between the maximum and minimum amplitude of the RF spectrum as a function of the pulse amplitude for a fixed pulse width of 1 μs and duty cycle of 1% (circles). The line gives the trend and is intended to guide the eye.

3.2. RF spectrum

The measurements of the spectrally dispersed NF allowed us to investigate the spectral evolution from modal to incoherent emission. However, due to their spectral resolution being limited to approximately 20 GHz, further in-depth spectral analysis is necessary. To verify whether there are still modes underlying the parabola-shaped spectra of Fig. 4 which are not resolved in the spectrally dispersed NF, we have measured the RF spectrum of the total intensity fluctuations for different driving conditions. For modal emission we expect peaks to appear in the RF spectrum due to beating between different transverse modes, each having a slightly different wavelength. This way we can identify the presence of transverse modes with frequency differences down to the resolution bandwidth of the electrical spectrum analyzer (which was set to 1 MHz). When pulsing a VCSEL, the wavelength will dynamically evolve (exhibiting a so-called frequency chirp). However, as we do not measure the emission wavelength but rather wavelength differences in the RF spectrum, the beat notes will not be washed out completely by this dynamic wavelength shift because it chirps all modes simultaneously.

We measure the RF spectrum using a 12 GHz photodiode (*1554-B, NewFocus*) coupled via an amplifier (18 dB gain, 20 GHz bandwidth, *1422, NewFocus*) to an electrical spectrum analyzer (30 GHz bandwidth, *MS266C, Anritsu*). As the duty cycle of the pulses we apply is only 1%, we get a very small signal ($\approx$ 2dB above noise floor) if we measure the RF spectrum directly. In order to resolve the RF spectrum from the noise background, but also to measure the spectrum at different positions during a pulse, we use the gating capabilities of the electrical spectrum analyzer. That way, the spectrum will only be measured during the gate window (set to its minimum of 2 μs) after a trigger from the pulse driver has arrived. Both the resolution bandwidth and the video bandwidth of the electrical spectrum analyzer are set to 1 MHz as a compromise between high spectral resolution and high signal-to-noise ratio. For these settings, the time to measure one frequency component of the spectrum is 3 μs. Therefore, only one frequency component will be measured each time the gating window is open. Because of the minimum gate length of 2 μs, we are not able to measure the RF spectrum for pulses much shorter than 2 μs. Nevertheless, we can select different temporal positions within longer pulses by changing the delay of the trigger signal.

In Fig. 6 (left) we show the measured RF spectrum for CW and pulsed driving conditions.

#89583 - $15.00 USD Received 9 Nov 2007; revised 8 Jan 2008; accepted 8 Jan 2008; published 18 Mar 2008

Multiple peaks are clearly visible for CW operation, showing that in CW a large number of transverse modes are excited. From the CW RF spectrum, we can also see that the frequency difference between neighboring transverse modes is smaller that the resolution of the optical spectrum shown in Fig. 3. When we drive the VCSEL with a pulse width of 1 μs, a duty cycle of 1% and an amplitude of 22 mA (see Fig. 6) we still observe peaks in the RF spectrum. This is in accordance with the structured, modal FF (not shown) that we observe at this pulse amplitude. If we increase the pulse amplitude further, the peaks completely disappear and we observe a flat, non-peaked RF spectrum (see Fig. 6 for a pulse amplitude of 145mA) for those driving conditions that generate a Gaussian FF.

The disappearance of the peaks in the RF spectrum is further quantified in Fig. 6 (right), where we plot the ratio of the maximum and minimum power in the RF spectrum as a function of the pulse amplitude (for a fixed pulse width of 1 μs). For a pulse amplitude smaller than 60 mA, the value in Fig. 6 (right) is larger than 10 dB and the RF spectrum contains large peaks indicating modal emission. The height of the peaks is not monotonically decreasing for amplitudes between 14 mA and 40 mA because the modal composition of the beam is changing when the pulse amplitude is changed. For amplitudes above 70 mA, the difference between the maximum and minimum in the RF spectrum becomes small (falling below 7 dB) indicating non-modal emission. The pulse amplitudes for which the peaks disappear in the RF spectrum coincide with those that result in a Gaussian FF. Moreover, the trend towards non-modal emission shown in Fig. 6 (right) is remarkably similar to the decrease of the coherence with increasing pulse amplitude reported in Fig. 4 of [10].

4. Temporally resolved spatial coherence

As stated before, we attribute the simultaneous appearance of the Gaussian FF, the parabola shaped spectrally dispersed NF and the flat RF spectrum to a loss of spatial coherence. To finally prove this, we directly characterize the transition to spatially incoherent emission by measuring the evolution of the NF spatial coherence. We do not measure the full spatial coherence function over the entire VCSEL aperture, but we use a pair of pinholes to select two positions in the imaged near field. The two pinholes are rectangular shaped with a size of 0.1 mm by 0.08 mm and have a center-to-center separation of 0.3 mm. The diameter of the imaged NF is 2.26 mm. Therefore, the magnification of the imaging setup is 45. The coherence radius that we extract from the measured FF divergence angle is 1.4 μm and the imaged coherence diameter is thus 0.126 mm. We have chosen the pinhole separation to be somewhat larger than the imaged coherence diameter (0.3 mm compared to 0.126 mm) such that the visibility of the interference fringes drops to almost zero in case of incoherent emission. The visibility of the resulting interference pattern is then used as a measure for the degree of spatial coherence.

Because of the low intensity of the interference patterns, we use a slow non-gated 12-bit camera (*UP-680, Uniq Vision*) in these measurements. Temporal resolution is now achieved by differential analysis [7] of the interference patterns observed for slightly different driving conditions. We supply to the VCSEL a pulse train of 40 ns long pulses with 40 ns separation between the pulses, which is the shortest pulse width we can generate with our driver. Between each consecutive pulse train, we switch the laser off for a longer time (typically 100 μs) such that the laser can cool down again before the next train of pulses is applied. Each pulse has the same amplitude. As the integration time of the camera is still much longer than the pulse train repetition time, the difference between the interference pattern for X pulses and for (X - 1) pulses gives us the average interference pattern for only the Xth pulse. The limitation of this differential technique is that we can only see the interference pattern averaged over many events.

Using this technique, we obtained the spatial coherence for different numbers of pulses in

#89583 - $15.00 USD Received 9 Nov 2007; revised 8 Jan 2008; accepted 8 Jan 2008; published 18 Mar 2008

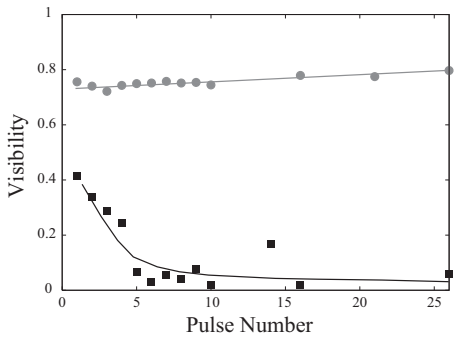

Fig. 7. Evolution of the degree of spatial coherence during a pulse train for a pulse amplitude of 22 mA (gray circles) and of 145 mA (black squares). The lines are only intended to guide the eye. The BA-VCSEL was operated in quasi-cw mode with pulse widths of 40 ns.

the pulse train. In Fig. 7 we plot the evolution of the spatial coherence for a pulse amplitudes of 22 mA and 145 mA. For low amplitudes (such as 22 mA), we know from the structured FF that the emission is modal and we see in Fig. 7 that the spatial coherence is high (exhibiting contrast values around 0.8) and stays almost constant. For high amplitudes (such as 145 mA), the FF transforms into a Gaussian profile during the first μs of emission. During this transition we see in Fig. 7 that the spatial coherence is strongly decreased (typically to below 0.1). As the amplitude is the same for each pulse, the injected current and the carrier density will also be the same for each pulse. Only thermal effects can spill over from one pulse to the next, indicating these thermal effects are essential to explain our measurements.

In case of incoherent emission, we have also observed that the visibility is independent of the pinhole pair's position in the imaged NF, showing that the coherence diameter is smaller than the pinhole separation over the entire VCSEL's aperture. For modal emission, we have observed that the visibility changes considerably if we change the position of the pinhole pair. In that case, the transverse modes being selected by the pinholes will change if we change the position of the pinholes, resulting in a change of the visibility as observed experimentally. The exact value of the visibility is difficult to predict, because many transverse modes are emitted simultaneously.

5. Evolution back to continuous-wave operation

So far we have mainly looked at the evolution within the first μs from modal to non-modal emission. But we also expect the opposite evolution to happen for longer pulse durations as CW operation is approached. Therefore, we have measured the emission properties for longer current pulses. Five single-shot measurements of the spectrally resolved NF intensity profiles for approximately 105 μs long current pulses are depicted in Fig. 8. At $\tau \sim 10$ μs, the spectrum still exhibits a parabola-like structure which was established at $\tau \sim 1$ μs (cf. Fig. 4). However, the shape is significantly modified at $\tau \sim 10$ μs. This is due to thermal effects discussed in detail in [15]. During the next 90 μs, Fig. 8 reveals a change from the parabola-like structure back towards well-defined transverse modes. These modes can already be identified around 80 μs after turn-on. The measurements therefore give evidence that transverse mode emission is re-established on a time-scale of a few tens of microseconds. The re-appearance of transverse modes can also be seen in the gated RF spectra. In Fig. 9 we show the RF spectra during a 145 mA pulse for different gating positions within the pulse length of 100 μs. At the beginning of the pulse, the RF spectrum is flat indicating that no transverse modes are present in the

#89583 - $15.00 USD Received 9 Nov 2007; revised 8 Jan 2008; accepted 8 Jan 2008; published 18 Mar 2008

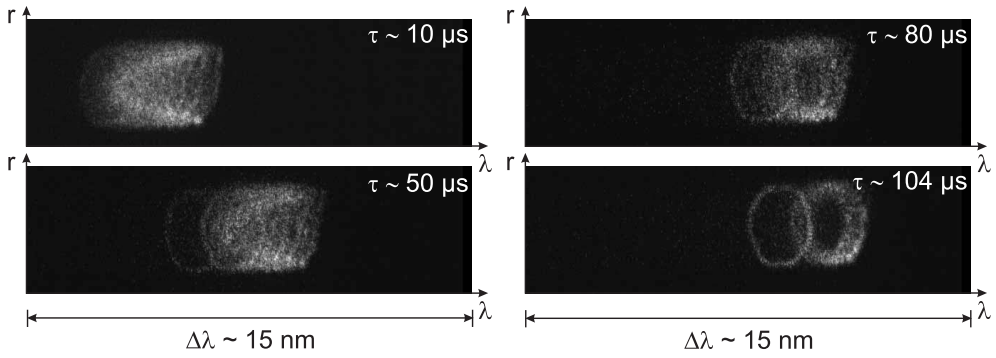

Fig. 8. Sequence of single-shot measurements of the BA-VCSEL's spectrally dispersed NF emission behavior. The BA-VCSEL was operated in quasi-cw mode with pulse widths of approximately 105 μs. The times denoted in the upper right corner of the images are the positions of the single-shot measurements after turn-on.

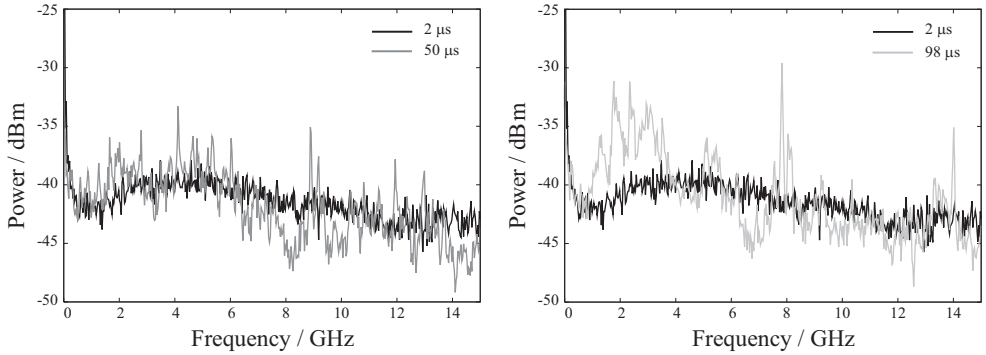

Fig. 9. RF spectrum of the emitted intensity at different temporal position within a 100 μs pulse with amplitude of 145 mA amplitude: at 2 μs (black), at 50 μs (dark gray) and at 98 μs (light gray). The noise floor of the measurement setup is at -58 dBm

emission. But after 50 μs, peaks due to transverse mode beating appear in the RF spectrum. At later times during the pulse, peaks remain visible in the RF spectrum but they shift in frequency as the modal composition of the emitted beam is still changing.

6. Discussion

The occurrence of the Gaussian FF profile described here coincides well with the operation conditions under which the Gaussian FF was observed in [10]. The measurements of the emission dynamics presented here give detailed insight into the evolution from modal to non-modal emission. We interpret the observed emission behavior as follows.

After the current pulse is switched on, the average temperature within the cavity increases due to Joule heating. The resulting thermal expansion of the cavity leads to the fast wavelength shift depicted in Fig. 5. Due to this fast thermal chirp, the BA-VCSEL's cavity is kept in a transient state with dynamically changing cavity conditions. However, the thermal chirp alone is not sufficient to prevent the build-up of cavity modes: though the thermal chirp is strongest during the first hundreds of nanoseconds of emission (cf. Fig. 5), the emission is still dominated by transverse modes indicated by the structured FF profile (cf. Fig. 2) and the distinguishable modes in the optical spectra (cf. Fig. 4). The evolution of the FF profile shown in Fig. 2 reveals

#89583 - $15.00 USD Received 9 Nov 2007; revised 8 Jan 2008; accepted 8 Jan 2008; published 18 Mar 2008

a reduction of the emission angle during the next hundreds of nanoseconds (see, $\tau \sim 0.3\ \mu$s). This reduction results from the formation of a thermal lens having the effect of an additional waveguide in the VCSEL-cavity. The particular shape of the thermal lens in the studied VCSEL is determined by the spatially inhomogeneous heating of the device resulting from the radially inhomogeneous current injection and optical emission because of the ring-shaped current contact [15]. As has been discussed in [16], a refractive index variation, e.g. due to a thermal lens, can lead to an increase in the modal build-up time. Therefore, the fast spatially inhomogeneous thermal chirp prevents the build-up of cavity modes and leads to the loss of spatial coherence. The Gaussian FF profile and the loss of modal emission is thus reached only after the inhomogeneous heating of the device has led to the formation of a strong enough thermal lens a few hundred nanoseconds after turn-on. The loss of spatial coherence can be observed as a loss of modal patterns in the FF profile (Fig. 2) and in the corresponding optical and RF spectra (Fig. 4 and Fig. 6). We can also directly observe this in the evolution of the NF spatial coherence (see Fig. 7) as the slit separation becomes larger than the coherence length when the modal emission is lost.

We can now assume that the BA-VCSEL lases in a superposition of independent "coherence islands" instead of in cavity modes as was introduced in [10]. Thus, the BA-VCSEL can be considered a quasi-homogeneous Schell-model source characterized by spatially incoherent emission and a Gaussian FF distribution. The characteristic parabola-like structure of the spectrally dispersed NF profile shown in Fig. 4, e.g. at $\tau \sim 1\ \mu$s, is a direct result of the inhomogeneous heating of the device and the emission in coherence islands. In [15], we have shown how information on the radial temperature distribution within the VCSEL-cavity can be extracted from a sequence of such optical spectra.

The explanations for the occurrence of the Gaussian FF profile and the loss of modal emission given above require that the observed phenomenon is a transient effect. This is confirmed by the measurements of the spectrally dispersed NF profiles depicted in Fig. 8 where the evolution back to modal emission is demonstrated for long current pulses. The incoherent emission is thus a transient regime, which lasts for several microseconds, but during this transient the FF divergence angle and the spatial coherence properties remain almost constant. Moreover, the measurements in Fig. 8 once again underline the connection between the spatial coherence shown in Fig. 7 and the spectral properties (modal or non-modal) of the BA-VCSEL's emission. During emission in transverse modes, the spatial coherence is high, whereas the parabola-like spectrum is associated with spatially incoherent (non-modal) emission [15].

7. Conclusions

We studied the evolution of a BA-VCSEL's emission towards the spatially incoherent state of emission discussed in [10]. The measurements show the onset of high order transverse modes shortly after turn-on. Heating of the device then leads to the formation of a thermal lens which increases the time for modes to build-up in the cavity. Additionally, the device experiences a fast thermal chirp, which in combination with the thermal lens, prevents the build-up of cavity modes. Our measurements show that the transition to incoherent emission occurs within the first microsecond of emission. The transition back to emission in well-defined transverse modes takes place around 100 μs after turn-on.

The measurements presented here further complement and verify our claim in [10] of obtaining spatially incoherent from a BA-VCSEL. In the incoherent emission regime, we observe a loss of modal patterns in the FF profile, in the optical spectra and in the RF-spectra. This leads to the formation of a Gaussian FF profile, which can be explained by considering the device as a quasi-homogeneous Schell model source. The optical spectra corresponding to the Gaussian FF profiles (and incoherent emission) are characterized by a parabolic structure. The appearance

#89583 - $15.00 USD Received 9 Nov 2007; revised 8 Jan 2008; accepted 8 Jan 2008; published 18 Mar 2008

of the Gaussian FF coincides with a drop in the NF spatial coherence.

The results presented here provide insight into the processes involved during the evolution of the emission. The emission properties may be harnessed for various applications where high output powers with low degree of spatial coherence are required. Possible applications for such a spatially incoherent light source may include illumination or utilization for projection beams, where the low spatial coherence of the emission might lead to a reduction in the speckle-contrast. Furthermore, our results might help to design laser structures suitable for spatially incoherent emission.

Acknowledgements

The authors are indebted to M. Grabherr of U.L.M.-Photonics for providing the devices. I. Fischer, M. Peeters and G. Verschaffelt acknowledge the IWT project 030501, the IAP P6/10 network "Photonics@be", the VUB-IOF project "Micro-photonics" and EU FP6/NEMO network for financial support.

#89583 - $15.00 USD Received 9 Nov 2007; revised 8 Jan 2008; accepted 8 Jan 2008; published 18 Mar 2008